Electrostatics and the Ion Selectivity of Ligand-Gated Channels

Charlotte Adcock, Graham R. Smith, and Mark S. P. Sansom
Laboratory of Molecular Biophysics, University of Oxford, Oxford OX1 3QU, England

ABSTRACT The nicotinic acetylcholine receptor (nAChR) is a cation-selective ion channel that opens in response to acetylcholine binding. The related glycine receptor (GlyR) is anion selective. The pore-lining domain of each protein may be modeled as a bundle of five parallel M2 helices. Models of the pore-lining domains of homopentameric nAChR and GlyR have been used in continuum electrostatics calculations to probe the origins of ion selectivity. Calculated pK_A values suggest that "rings" of acidic or basic side chains at the mouths of the nAChR or GlyR M2 helix bundles, respectively, may not be fully ionized. In particular, for the nAChR the ring of glutamate side chains at the extracellular mouth of the pore is predicted to be largely protonated at neutral pH, whereas those glutamate side chains in the intracellular and intermediate rings (at the opposite mouth of the pore) are predicted to be fully ionized. Inclusion of the other domains of each protein represented as an irregular cylindrical tube in which the M2 bundles are embedded suggests that both the M2 helices and the extramembrane domains play significant roles in determining ion selectivity.

INTRODUCTION

The ligand-gated ion channels (LGICs) are a superfamily of integral membrane proteins that mediate synaptic transmission (Barnard, 1992; Ortells and Lunt, 1995). The best characterized member of this family is the nicotinic acetylcholine receptor (nAChR) (Stroud et al., 1990; Lester, 1992; Hucho et al., 1996), which mediates neurotransmission at vertebrate neuromuscular junctions, in addition to playing a role at some synapses of the vertebrate central nervous system and in the nervous systems of invertebrates. Both functional and structural studies on nAChR indicate that it undergoes a conformational change upon binding of two neurotransmitter (acetylcholine) molecules, switching from a closed to an open state (Unwin, 1995). The open state allows passage of monovalent (and some divalent) cations through a pore that runs through the center of the protein. Other LGICs, such as the glycine receptor (GlyR) (Langosch et al., 1990), are permeable to anions rather than cations. Anion-selective LGICs mediate inhibitory neurotransmission, whereas cation selective LGICs are excitatory. Other members of the nAChR superfamily of LGIC include the anion-selective $GABA_A$ receptor (Macdonald and Olsen, 1994) and the cation-selective $5HT_3$ receptor (Jackson and Yakel, 1995) channels. Ionotropic glutamate receptor channels are believed to be rather more distantly related (Hollmann et al., 1994).

The members of the nAChR superfamily share common structural features. They are all formed by assemblies of five similar (or sometimes identical) subunits surrounding a central transbilayer pore. They are thought to share the same subunit architecture, with a large N-terminal extracellular (EC) domain, four putative transmembrane (TM) segments (M1 to M4), and an intracellular domain (IC) composed largely of the loop between M3 and M4 (see Fig. 1 *A*). A number of mutagenesis and chemical labeling studies indicate that the M2 segment forms the immediate lining of the transbilayer pore (Changeux et al., 1992; Lester, 1992). Indeed, peptide fragments corresponding to M2 segments spontaneously adopt an α-helical conformation and self-assemble to form ion channels in lipid bilayers (Langosch et al., 1991; Montal, 1995). There is some debate about the secondary structure of the M1, M3, and M4 segments (Hucho et al., 1994). However, the patterns of labeling and of mutation effects strongly suggest that the M2 segments are α-helical. Cryoelectron microscopy has been used to image *Torpedo* nAChR at 9-Å resolution in both its open and closed states (Unwin, 1993, 1995). Both studies reveal density corresponding to five kinked α-helices surrounding the central transmembrane pore, which are thus believed to be the M2 α-helices.

In an earlier study we have used molecular dynamics simulations subject to restraints derived from cryoelectron microscopy and mutagenesis data to generate atomic resolution models of the M2 α-helix bundle that forms the inner lining of the nAChR pore (Sansom et al., 1995; Sankararamakrishnan et al., 1996). In this paper we extend these modeling studies to the pore of a GlyR, and use continuum electrostatics calculations to analyze the roles of the ionizable side chains in M2 α-helix bundles and of the remainder of the nAChR and GlyR protein molecules in determining the ion selectivity of LGICs.

Received for publication 22 December 1997 and in final form 9 June 1998.

Address reprint requests to Dr. Mark S. P. Sansom, Laboratory of Molecular Biophysics, The Rex Richards Building, University of Oxford, South Parks Road, Oxford OX1 3QU, England. Tel.: +44-1865-275371; Fax: +44-1865-510454; E-mail: mark@biop.ox.ac.uk.

0006-3495/98/09/1211/12 $2.00

METHODS

Programs

Restrained molecular dynamics simulations were carried out using Xplor V3.1 (Brünger, 1992) with the Charmm param19 parameter set (Brooks et al., 1983). Only polar hydrogens were treated explicitly, i.e., apolar groups were represented as extended atoms. All electrostatics calculations em-

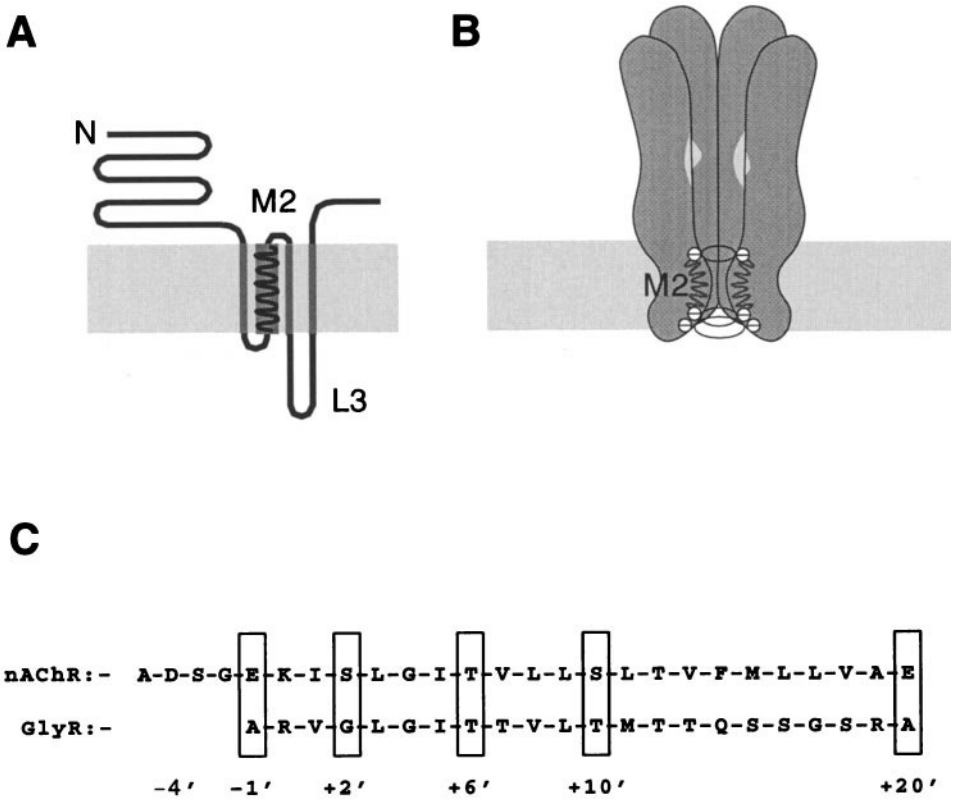

FIGURE 1 (*A*) Proposed topology of a single LGIC subunit. The extracellular N-terminal domain is followed by four TM segments. The M2 segment, which adopts an α-helical conformation, and the extensive intracellular loop (L3) between M3 and M4 are labeled. (*B*) Schematic diagram of the overall structure of the nAChR. The foremost subunit of the pentameric assembly is omitted. The approximate position of the M2 helices and of the three rings of acidic sidechains are indicated. (*C*) Sequences of nAChR α7 and GlyR α1 M2 α-helices, extending from residue $-5'$ to $+20'$ (using the numbering scheme of, e.g., Lester (1992) for the nAChR and from $-1'$ to $+20'$ for the GlyR (see text). For the nAChR, M2 models run from $-1'$ to $+20'$ and M2-extended models from $-5'$ to $+20'$. The proposed pore-lining side chains at positions $-1'$, $+2'$, $+6'$, $+10'$, and $+20'$ are highlighted.

ployed UHBD version 5.1 (Davis et al., 1991) (with some local modifications) and partial atomic charges from the Quanta/Charmm22 parameter set. Ribbon diagrams of molecules were created using Molscript (Kraulis, 1991). Pore lining diagrams were generated using PORELINING (Smith and Adcock, unpublished work). Rasmol was used for visualization of models and production of cylinder diagrams. All calculations and simulations were carried out on Silicon Graphics workstations. Quanta 4.1 (MSI) and Charmm were used in the generation of the simplified cylinder model. Memsat (Jones et al., 1994) was used to define transmembrane regions of LGIC subunit sequences.

Generation of M2 models

Our implementation of simulated annealing via restrained molecular dynamics has already been described in detail (Kerr et al., 1994; Sansom et al., 1995). To summarize, a two-stage protocol is used. In the first stage a simulated annealing protocol (Nilges and Brünger, 1993) is used to "grow" the atoms of a model out from a fixed predefined Cα template, corresponding to a parallel bundle of idealized α-helices. In the second stage all atoms are free to move subject to harmonic distance restraints. These restraints are of three types: target (positional) restraints, and two classes of distance restraint, one intrahelix and one interhelix. Target restraints are used to restrain the M2 α-helices to their approximate positions as defined by the 9-Å resolution electron microscopic image of the pore (Unwin, 1995). Intrahelix restraints are imposed to maintain the hydrogen bonding pattern of each M2 α-helix. Interhelix restraints are used to orient pore-lining side chains toward the center of the helix bundle.

Electrostatic profiles

Electrostatic potential ($F\Phi$) was calculated by solving the Poisson-Boltzmann equation:

$$\nabla \cdot \epsilon(\mathbf{r})\nabla\Phi(\mathbf{r}) - \kappa'^2\sinh(\Phi(\mathbf{r})) = -4\pi\rho(\mathbf{r})$$

where $\Phi(\mathbf{r})$, $\epsilon(\mathbf{r})$, and $\rho(\mathbf{r})$ are the electrostatic potential, dielectric constant, and charge density, respectively, at position $\mathbf{r}$. The Debye-Huckel parameter, κ', is derived from the Debye length and hence from the ionic strength. The above form of the Poisson-Boltzmann equation is the full (i.e., nonlinear) form. In this study the linearized approximation was used (see Discussion). The continuum system used in all electrostatics calculations consisted of a low dielectric slab of thickness ~40 Å into which the protein models were inserted. The slab was generated from dummy atoms on a simple cubic lattice with a 2.5-Å spacing. The protein and low dielectric slab volume were defined by the solvent-accessible surface, and the volume was assigned a dielectric of 4. Both the dielectric inside the model pore representing solvent and the bulk solvent surrounding the low dielectric slab were set at 78 (unless stated otherwise in the main text). An ionic strength of 100 mM and a Stern radius of 2 Å were used.

pK_A calculations

To estimate the pK_As of these ionizable side chains in situ, established methods (Bashford and Karplus, 1990; Yang et al., 1993) via numerical solution of the linearized Poisson-Boltzmann equation were employed. These methods are based on calculating the difference between the electrostatic energy of an amino acid residue within its protein environment relative to its electrostatic energy when isolated in solution, for both protonation states of that residue. Similar methods have been applied to the acidic and basic side chains that form the narrowest region of the pore in bacterial porins (Karshikoff et al., 1994) and to the ionizable groups within bacteriorhodopsin (Bashford and Gerwert, 1992). There are two stages to the procedure. The first stage involves calculating the following free energy differences: 1) ΔG_1, the change in electrostatic free energy on transferring an isolated, unprotonated amino acid from water to its protein/water environment; and 2) ΔG_2, the change on transferring the same amino acid in its protonated state from water to its protein/water environment. Both free energies contain terms for 1) the interaction of the amino acid with its dielectric environment, calculated as a Born energy, ΔG_{BORN}; and

2) the electrostatic interaction of the amino acid with the partial atomic charges of the protein, while assuming that all other ionizable residues of the protein are in their un-ionized state, giving ΔG_{BACK}. Thus:

$$\Delta G_1 = \Delta G_{BORN}(PR) - \Delta G_{BORN}(R) + \Delta G_{BACK}(PR)$$

and

$$\Delta G_2 = \Delta G_{BORN}(PRH) - \Delta G_{BORN}(RH) + \Delta G_{BACK}(PRH)$$

where R is the unprotonated residue in isolation in water, PR is the unprotonated residue in the protein, RH is the protonated residue in isolation in water, and PRH is the protonated residue in the protein. The intrinsic pK_A of the amino acid in its protein environment is then given by

$$pK_{A,INTRINSIC} = pK_{A,MODEL} + \frac{1}{2.303}[\Delta G_1 - \Delta G_2]$$

where $pK_{A,MODEL}$ is the pK_A of the isolated amino acid. The intrinsic pK_A thus takes into account the effect of the dielectric and partial atomic charge environments of the protein within which an ionizable side chain finds itself, but does not take account of the ionization states of all other such side chains within the protein. In the second stage of the calculation, titration curves are calculated for all N ionizable residues within the protein, allowing absolute pK_A values to be measured. The latter were obtained via calculation of

$$p(\mathbf{x}) \propto \exp\left[-\ln 10 \sum_i \gamma_i (pK_{A,INTRINSIC,i} - pH) - \beta \sum_i \sum_{k<i} \Delta G_{i,k} \right]$$

where $p(x)$ is the probability of a residue existing in its ionized state and $\mathbf{x}$ is an N-element state vector whose elements are 0 or 1, depending on whether the residue is un-ionized or ionized, respectively, where $\gamma = -1$ for a basic residue, $\gamma = +1$ for an acidic residue, $\beta = 1/RT$, and $\Delta G_{i,k}$ is the screened Coulombic interaction energy between pairs of ionizable residues i and k (Bashford and Karplus, 1991; Lim et al., 1991).

The irregular cylinder model

An irregular cylinder model for the remainder of the channel protein (i.e., those regions of the protein other than the M2 helix bundle) was generated from a simple cubic lattice of atoms with a spacing of 2.5 Å. The dimensions of the irregular cylinder were determined from published electron microscopic images of the *Torpedo* nAChR in Toyoshima and Unwin (1988) and Unwin (1993, 1995). Net charges on the relevant domains (extracellular, transmembrane, versus intracellular) were calculated from the primary sequences of each subunit, excluding the M2 sequence and assuming full ionization of acidic and basic side chains, other than histidine, for which a charge of +0.5 was used. Charges on each region were distributed evenly over the dummy atoms forming the inner/outer surfaces of each cylinder. Calculations including an embedded M2 α-helix bundle were performed, using a model in which the bundle was inserted into the TM region of its corresponding cylinder model, discarding any cylinder atoms that were too close to M2 atoms.

RESULTS AND DISCUSSION

M2 α-helix bundle models

M2 α-helix bundle models were generated for two sequences: that of the chick neuronal α7 nAChR (Couturier et al., 1990) and that of the human α1 GlyR (Grenningloh et al., 1990). These two receptors were chosen as both are homopentameric in vitro (Couturier et al., 1990; Morr et al., 1995), which considerably simplifies modeling, as fivefold symmetry of the helix conformations and orientations may be assumed. The M2 sequences of α7 nAChR and α1 GlyR are compared in Fig. 1 *C*. The numbering scheme used throughout this paper is that of Lester (1992), in which the N-terminal (intracellular) glutamate of the nAChR M2 is E $-1'$ and the C-terminal (extracellular) residue is E $+20'$. Note that this is the same convention used by Smith and Sansom (1997b), but it differs from that used by Sankararamakrishnan et al. (1996), in which the same two residues were numbered E $+1'$ and E $+22'$, respectively. In the nAChR sequence M2 begins and ends with glutamate residues, whereas in the GlyR there are arginine residues close to both termini. Both sequences contain a number of hydroxyl-containing side chains. The hydroxyl-containing side chain at position $+2'$ of M2 (see Fig. 1 *B*) has been implicated in forming the lining of the narrowest region of the nAChR pore (Villarroel et al., 1991).

Models of pentameric M2 α-helix bundles were generated using simulated annealing/molecular dynamics (SA/MD) as described previously (Sankararamakrishnan et al., 1996; Sansom et al., 1995). In this procedure the α-helix kinks and positions are dictated by target restraints derived from the cryoelectron microscopy images (Unwin, 1993, 1995). The helix orientations by rotation about their long axes are determined by distance restraints between the Cβ atoms of residues $+2'$, $+6'$ and $+10'$, which have been shown in the case of the nAChR to line the pore of the open state of the receptor channel (Changeux et al., 1992; Lester, 1992; Hucho et al., 1996). These restraints orient these side chains toward the pore lumen. The sensitivity of the SA/MD procedure to the initial orientation assumed for the M2 α-helices was tested by rotating the starting Cα templates for these helices about their long axes by $\pm 10°$ to either side of the optimum value. The resultant structures did not differ significantly in their electrostatic or geometric properties from structures without such an initial displacement. In generating the GlyR M2α1 model by SA/MD, it is assumed that the pore architecture of the GlyR is similar to that of the nAChR. In the absence of definitive structural data, this is justified by the significant sequence homology between nAChR and GlyR sequences, and by the functional similarities between these two families of receptor channels (Betz, 1990).

The pore-lining side chains in the two models are compared in Fig. 2. It can be seen that both mouths of the nAChR M2α7 pore are lined by rings of glutamate residues (E $-1'$ and E $+20'$) (Changeux et al., 1992). There is a strip of hydroxyl-containing residues (S $+2'$, T $+6'$, and S $+10'$) along the N-terminal pore-lining face of each helix. These residues are conserved within the various nAChR sequences. In contrast, the GlyR M2α1 pore has rings of arginine side chains (R0′ and R $+19'$) close to both mouths.

The radius profiles of both the nAChR M2α7 and GlyR M2α1 pores were calculated. They were similar, with the

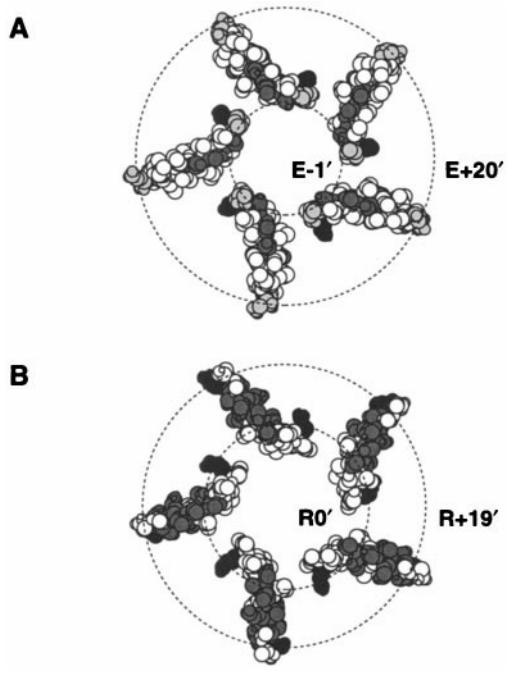

FIGURE 2 Pore-lining side chains of the (*A*) nAChR and (*B*) GlyR M2 pore models. The diagrams are generated by projecting the inner surfaces of the M2 helices onto a plane. The projection used is comparable to peeling back the constituent helices like the petals of a flower, such that the innermost residues of the pore lining are uppermost in the projection. Thus the N-termini of the helices form the innermost ring and the C-termini the outermost ring of the diagrams. The gray scale encodes the residues as follows: dark grey, basic; mid-grey, polar, uncharged; light grey, acidic; white, hydrophobic. In *A* (nAChR) the two broken circles represent the rings of glutamate side chains at the N-terminal (E −1′) and C-terminal (E +20′) mouths of the pore. In *B* (GlyR) the two broken circles represent the rings of arginine side chains close to the N-terminal (R0′) and C-terminal (R +19′) mouths of the pore.

narrowest region of the pore being situated toward the N-terminal mouth and having a radius of ~6 Å in the vicinity of residue 2′. As has been discussed previously (Sankararamakrishnan et al., 1996), this is consistent with estimates of the minimum pore radius based on electrophysiological measurements of the largest organic cation able to permeate nAChR (Dwyer et al., 1980; Nutter and Adams, 1995) and GlyR (Bormann et al., 1987), provided one takes into account the presence of an "annulus" of low-mobility water in the narrowest region of the pore, as indicated by MD simulations on nAChR M2α7 helix bundles (Smith and Sansom, 1997b).

Electrostatic potential profiles

As a first step toward understanding ion selectivity, one may compute electrostatic potential energy profiles along the M2 pore axis (z) via numerical solution of the linearized Poisson-Boltzmann equation. To approximate the dielectric effect of the other transmembrane segments around M2 and the surrounding lipid bilayer, the M2 α-helix bundles were embedded in ~40-Å-thick "slabs" of low dielectric before electrostatic potentials (Φ; see Methods) were calculated. Electrostatic potential profiles are displayed as $F\Phi$ versus z, where F is Faraday's constant. Thus they represent the potential energy (in kcal/mol) of a univalent cation in the channel, apart from the effect of the cation's repulsive interaction with its own polarization charge (Hoyles et al., 1996). The latter term is likely to be small because the cation is shielded by counterions. However, the magnitude of such screening is difficult to estimate with any degree of accuracy, given the uncertainties about the true concentration of counterions within the pore. The profiles for the nAChR M2α7 and GlyR M2α1 bundles are compared in Fig. 3. It can be seen that the nAChR M2α7 profile shows a potential well of depth ~$3RT$ toward the C-terminal mouth of the pore. This corresponds to the ring of E +20′

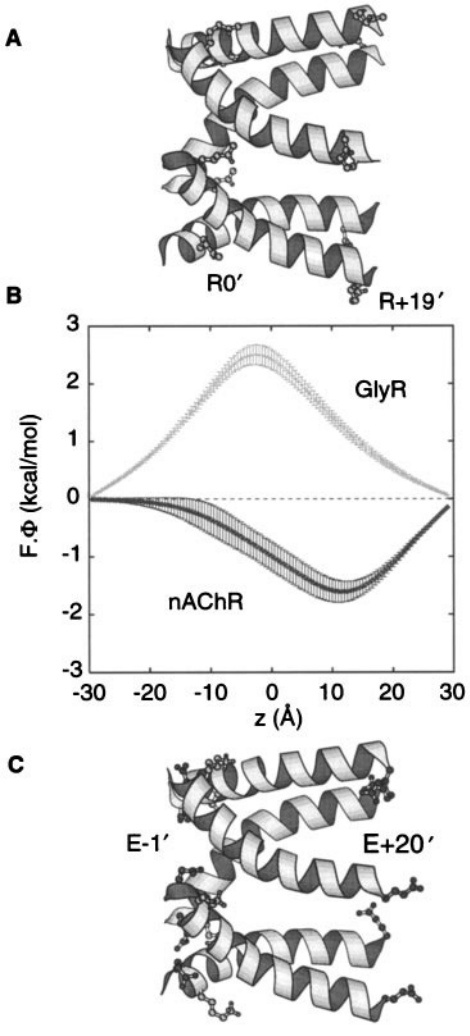

FIGURE 3 Electrostatic potential ($F\Phi$) profiles (*B*) for the GlyR (*gray curve*) and nAChR (*black curve*) M2 pore models. The error bars represent standard deviations from averages taken across the members of each ensemble of 25 structures. The corresponding GlyR (*A*) and nAChR (*C*) M2 pore models are shown, viewed perpendicular to the pore axis, with their intracellular mouths (N-termini) on the left-hand side. The diagrams, drawn using Molscript (Kraulis, 1991), are approximately aligned with the z axis in *B*.

side chains. The effect of the ring of E −1′ side chains seems to be largely canceled out by the presence of the adjacent K0′ and by the N-terminal component of the α-helix dipole (Hol et al., 1978). In contrast, the GlyR M2α1 profile has a potential barrier close to the middle of the pore, of height ~4*RT*. This barrier is thus approximately midway between the two rings of arginine side chains. The presence of a well in the nAChR profile and a barrier in the GlyR profile is consistent with the observed cation selectivity of nAChR and anion selectivity of GlyR. The "error" bars on the potential profiles reflect the variation in profiles between different members of the same ensemble of structures. It is evident that the variations within each ensemble are insignificant compared with the difference between the nAChR M2α7 and GlyR M2α1 ensembles.

pK_A values of ionizable side chains

A simplifying assumption is implicit in the electrostatic potential energy calculations just discussed, namely that all acidic and basic side chains are in their fully ionized state. However, the protein environment of an ionizable residue can significantly change its pK_A value relative to that of isolated residue in aqueous solution. In the case of the rings of ionizable side chains at either mouth of the M2 bundle models, their environment differs significantly from that of a dilute aqueous solution in two respects. First, the side chains are sitting in a solvent-filled pore surrounded by low dielectric (protein and "bilayer"). Second, the individual members of a ring are relatively close to one another (~12 Å at their closest for the E +20′ rings) and thus interact electrostatically with one another to an appreciable extent. Furthermore, their location at the C-terminus of the α-helix means that the helix dipole will tend to destabilize the deprotonated (i.e., negatively charged) state of the E +20′ side chains, thus raising their pK_As.

Absolute pK_A values were calculated (see Methods) for all 15 ionizable residues in the nAChR M2α7 bundle, i.e., the three rings E −1′, K0′, and E +20′, each of which contains five ionizable side chains, and for the corresponding two rings (R0′ and R +19′) of the GlyR M2α1 (Table 1). From analysis of a single in vacuo structure (i.e., a structure as generated by in vacuo SA/MD) of the nAChR M2α7 ensemble, it is evident that the two rings of glutamate side chains behave rather differently form one another. The mean absolute pK_A for E −1′ is considerably lower than the value for an isolated glutamic acid (4.4; Nazaki and Tanford, 1967). This shift in pK_A arises from the location of E −1′ at the N-terminus of the M2 helix, thus differentially stabilizing the negatively charged ionized form by interaction with the helix macrodipole, and from the presence of the adjacent K0′ side chain with which E −1′ forms an ion pair interaction in most structures from the ensemble. In contrast, the mean absolute pK_A of E +20′ is significantly higher than that of an isolated glutamate residue. This is a consequence of the location of E +20′ at the C-terminal end of the helix macrodipole and the fact that the E +20′ side chains, if all ionized, would experience unfavorable electrostatic interactions with one another across the lumen of the pore.

To estimate the importance of the helix dipole effect, similar calculations were performed on a 22-residue α-helix made up entirely of alanine residues apart from a single "guest" glutamate residue. The calculated pK_A of the glutamate residue shifted from ~3 at the N-terminus to ~6 at the C-terminus. This is in agreement with a number of experimental studies of shifts in pK_As of groups located at the ends of helices (Huyghues-Despointes et al., 1993; Sitkoff et al., 1994).

To estimate the robustness of this result to the model structure, a number of additional calculations were performed (Table 1). Repeating the same calculation for a further four in vacuo nAChR M2α7 structures yielded average pK_A values across all five structures, which supported the same general conclusions. Electrostatics calculations were also performed on an nAChR M2α7 model that had been "refined" by a 200-ps MD simulation in the presence of TIP3P water molecules within and at either mouth of the pore (Smith and Sansom, 1997b), to relax the conformations of the side chains. Again, this suggested a similar qualitative difference between the E −1′ and E +20′ side chains in terms of their pK_As. The effect of assuming a lower value of the dielectric for water within the pore was examined. Previous MD simulation studies (Sansom et al., 1997) suggested that water confined within a pore made up of approximately parallel α-helices exhibits a lower dielectric than does bulk water, because of dielectric saturation of the water by the strong helix dipole field. Using a value of $\epsilon_{PORE} = 30$ for the dielectric within the pore and repeating the pK_A calculations with an in vacuo structure yields results similar to those from the calculation based on the same structure, but with $\epsilon_{PORE} = 78$. Finally, the effect of assuming zero ionic strength was tested. This again yielded similar results. Thus it seems that the general pattern of pK_A values for the nAChR M2α7 model does not depend much on the exact structure used or on some of the assumptions made in the electrostatics calculation. On this basis, it may be assumed that the E −1′ and K0′ side chain rings would be fully ionized, but that the fractional ionization of the E +20′ would be ~0.2 (for an absolute pK_A of ~7.5).

The consequences of this in terms of the electrostatic potential profile are illustrated in Fig. 4 *B*. It can be seen that assuming a fractional ionization of 0.2 for the E +20′ ring (i.e., only one of the five side chains ionized) results in the depth of the potential well being reduced from ~3*RT* to *RT*. Thus perturbation of pK_A values by the local protein environment is clearly an important factor to be taken into account when assessing the role of rings of ionizable side chains in ion selectivity.

If one repeats such calculations for the GlyR M2α1 model, then it can be seen (Table 1) that the C-terminal ring of arginines is likely to remain ionized, despite its location in a relatively low dielectric environment. Interestingly (if

TABLE 1 pK_A values for ionizable residues of M2 bundles

Models*	pK_A values#			
nAChR	D−4′	E−1′	K0′	E+20′
M2α7, single in vacuo structure, $\epsilon_{PORE} = 78$		−7.6 (±5.8)	13.7 (±5.9)	7.4 (±0.2)
M2α7, single in vacuo structure, $\epsilon_{PORE} = 30$		−7.7 (±5.9)	13.9 (±6.0)	8.1 (±0.4)
M2α7, single in vacuo structure, zero ionic strength		−8.2 (±5.9)	14.6 (±6.3)	8.2 (±0.3)
M2α7, five in vacuo structures		−3.6 (±4.9)	10.6 (±4.7)	7.8 (±1.4)
M2α7, single solvated structure		−11.0 (±1.6)	19.7 (±1.8)	7.1 (±1.0)
M2α7 + irregular cylinder (not charged)		−2.3 (±3.7)	6.0 (±4.0)	12.7 (±2.1)
M2α7 + irregular cylinder (charged)		2.9 (±3.1)	11.6 (±2.7)	16.6 (±2.7)
M2α7-extended, single in vacuo structure	−1.5 (±2.5)	0.8 (±4.2)	16.7 (±3.9)	7.0 (±0.4)
M2α7-extended + irregular cylinder (not charged)	−8.9 (±4.5)	0.6 (±4.7)	26.9 (±6.1)	10.3 (±2.2)
M2α7-extended + irregular cylinder (charged)	−6.1 (±4.5)	2.9 (±4.7)	30.2 (±6.1)	12.3 (±2.8)
GlyR M2α1			R0′	R+19′
M2α1, single in vacuo structure			6.6 (±2.1)	12.6 (±1.9)
M2α1 + irregular cylinder (not charged)			3.5 (±2.8)	11.4 (±1.5)
M2α1 + irregular cylinder (charged)			−5.2 (±3.2)	10.2 (±1.6)

*The in vacuo structures are those from SA/MD. The solvated structure is that from SA/MD "refined" by 200 pS of MD with TIP3P water molecules within and at either mouth of the M2 pore. In the case of the $\epsilon_{PORE} = 30$ model, the dielectric of the solvent region within the pore was set to 30; in all other calculations it was the same as for the bulk solvent, i.e., 78. M2α7-extended refers to those nAChR models with the four-residue N-terminal extension of the M2 helix. With respect to the models embedded within the irregular cylinder model of the remainder of the protein, "charged" and "not charged" refer to whether or not an average surface charge was applied to the cylinder (see text for details).

#The values given are for absolute pK_As (see text).

not unexpectedly), the more N-terminal arginine ring (R0′) exhibits a lower pK_A value, reflecting the unfavorable interaction of the helix macrodipole with the protonated side chain. Our calculations suggest that some of the Arg side chains in the N-terminal ring may therefore deprotonate. However, in this case it is possible that inclusion of other regions of the protein might reverse this conclusion, as there is an aspartate just a few residues N-terminal to R0′ in the sequence of α1 GlyR, which may form an ion pair with the arginine, thus favoring the protonated state of the latter residue.

It should be noted that in our current model, the M2 α-helices are not closely packed at their C-termini. It is likely that in the intact protein the spaces in between may be occupied by other residues. Experimental data suggest that the M1 transmembrane segment may also contribute to the pore lining in this region. Tentative models with part of the M1 segment built in an extended conformation between the C-termini of the M2 α-helices were constructed to be in agreement with Cys-scanning mutagenesis and photolabeling data (Akabas et al., 1994; DiPaola et al., 1990). The residues of M1 in the vicinity of E +20′ are all hydrophobic with the exception of a tyrosine, and preliminary calculations suggest that M1 would not cause a large shift in our calculated pK_A values. Of course, it cannot be ruled out that the effects of residues in the M2-M3 loop could alter pK_As.

The suggestion that some of the E +20′ side chains may be protonated finds support in the demonstration that mutation of residues in the E +20′ ring to neutral groups does not produce the linear change in current-voltage curves that would be expected if all of the glutamate side chains were in their deprotonated state (Kienker et al., 1994a). Furthermore, it has been shown that negatively charged sulphydryl-directed reagents may access cysteine side chains inserted into the pore on the N-terminal side of the (extracellular) E +20′ ring (Akabas et al., 1994), which again would be consistent with a protonated state for the latter. Interestingly, in muscle-type nAChR (including that of *Torpedo*) the heteropentameric nature of the channel means that the extracellular ring contains three acidic (two E and one D) and two neutral (two Q) side chains, which would be expected to produce a total charge similar to that achieved by the partial protonation of this ring in the homopentameric α7 nAChR. Preliminary models and calculations for a *Torpedo* nAChR M2 helix bundle yield pK_A values above 6.5 for the +20′ glutamate and aspartate side chains.

Extending the M2 helices

As there is experimental evidence which suggests that a further ring of acidic residues preceding the N-terminus of M2 in the amino acid sequence may play a role in channel selectivity (Galzi et al., 1992; Imoto et al., 1988), we have also explored a model of an M2α7 bundle in which the α-helices were extended by four residues at their N-termini (i.e., to residue −5′; see Figs. 1 *C* and 5 *A*), thus adding a further acidic residue at D − 4′. Computation of electrostatic potential profiles for these extended models suggested that addition of this residue resulted in a broader $F\Phi$ well extending further along the length of the model pore (see Fig. 5 *B*). Calculation of pK_A values for this nAChR M2α7-extended model (Table 1) suggests that the most likely ionization state will be 1) D −4′, fully ionized; 2) E −1′, fully ionized; 3) K^+0', fully ionized; and 4) E +20′, 50% ionized. Thus this calculation suggests that the influence of the nAChR M2α7-extended pore on the ion selectivity of the channel resides more at the intracellular than at the extracellular mouth.

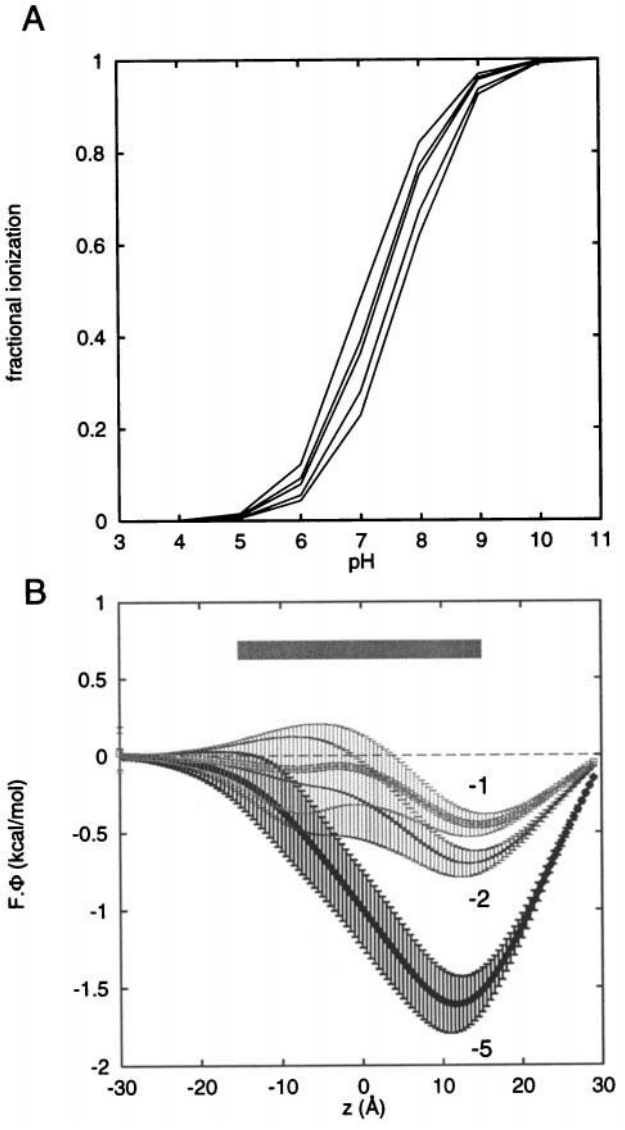

FIGURE 4 (*A*) Titration curves for the E +20′ side chains of a nAChR M2 pore model. A separate curve is shown for each of the five side chains. The mean pK_A is 7.4 (see Table 1). (*B*) Electrostatic potential ($F\Phi$) profiles for the nAChR M2 pore model, assuming that: all five (− 5, *bold black*); only two (− 2, *thin black*); or one (− 1, *gray*) of the E +20′ side chains are ionized. The solid gray bar above the curves indicates the approximate extent (on *z*) of the M2 helix bundle model.

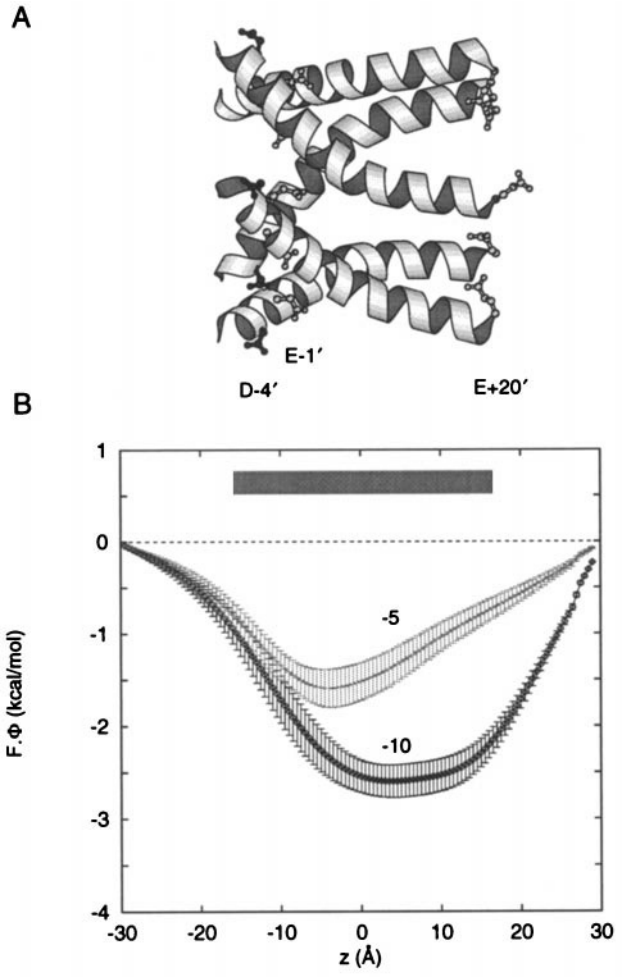

FIGURE 5 nAChR M2-extended model. (*A*) The extended pore model, viewed perpendicular to the pore axis, with its intracellular mouth (N-termini) on the left-hand side. The D −4′ side chains are shown in dark gray and the E −1′ and E +20′ side chains in pale gray. (*B*) The electrostatic potential profiles for the same model, with either all ionizable residues in their default charge states (−10, *black*) or the most likely ionization state, with the E +20′ side chains fully protonated (−5, *gray*).

The remainder of the molecule: a simple model

The M2 region is unlikely to be the only region that influences the selectivity of LGICs. Indeed, as discussed by (Unwin, 1989), it seems likely that the distribution of charge elsewhere on the surface of the channel molecule may influence the selectivity of the channel through an electrostatic mechanism. To address this question, a simple model of the remainder (i.e., the non-M2 region) of a LGIC molecule was constructed, taking into account the low-resolution envelope of the nAChR as a whole, as determined by cryoelectron microscopy (Toyoshima and Unwin, 1988).

The simple model of the LGIC consists of an irregular cylinder of pseudoatoms, with dimensions matching those derived from low-resolution cryoelectron microscopy (Fig. 6 *A*). Thus the cylinder is 110 Å long, with an inner radius of 10 Å and an outer radius of 30 Å. The intracellular (IC) section runs from $z = -35$ to -15 Å, the transmembrane (TM) section from $z = -15$ to $+15$ Å, and the extracellular (EC) section from $z = +15$ to 75 Å. The same dimensions were used for the simplified models representing the nAChR α7 and the GlyR α1. Of course, the exact distribution of charge within these domains is unknown. However, based on the proposed topology of the LGICs (Fig. 1 *A*) and their sequences, it is possible to evaluate the net charges in the IC, TM, and EC regions. For the α7 nAChR these are as follows: IC, $\Sigma q = +2.5$e; TM, $\Sigma q = -5.0$e; and EC, $\Sigma q = -17.5$e (where the charges are per channel, i.e., per pentamer). For the α1 GlyR these are as follows: IC, $\Sigma q = +62.5$e; TM, $\Sigma q = -5.0$e; and EC, $\Sigma q = -2.5$e. Note that residues within the M2 α-helices were excluded from this

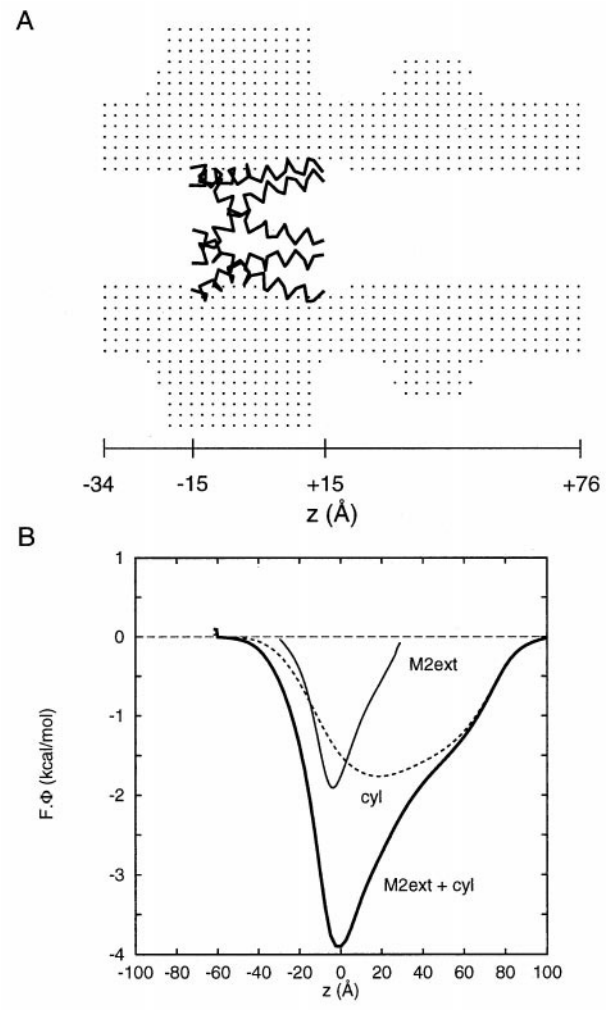

FIGURE 6 (*A*) nAChR M2α7-extended pore model (Cα traces in *black*) embedded within an irregular cylinder model of the remainder of the protein plus a slab model of the bilayer (*gray dots*). (*B*) Electrostatic potential ($F\Phi$) profiles for nAChR M2α7-extended pore and irregular cylinder models: M2α7-extended model (no irregular cylinder) in its most likely ionization state (*thin solid line*); irregular cylinder model (no M2 helix bundle), with the net charge spread over both the inner and outer surfaces of the cylinder (*broken line*); M2α7-extended model embedded in the irregular cylinder model (*bold solid line*). The intracellular domain of the irregular cylinder extends from $z \approx -35$ to -15 Å; the transmembrane domain from $z \approx -15$ to $+15$ Å; and the extracellular domain from $z \approx +15$ to $+75$ Å.

calculation for the TM region. In these calculations charges of $+1$ for all Lys and Arg, -1 for all Glu and Asp, and 0.5 for all His residues are assumed. As noted by, e.g., Unwin (1989) for the cation-selective nAChR M2α7, there is a negative net charge in the EC segment, whereas for the GlyR M2α1 there is a positive net charge in the IC segment that is made up of the extended loop between the M3 and M4 TM segments. It is further assumed that the charged residues are present on the surface of the cylinder, and that the charge is spread equally over the inner and outer surfaces of the cylinder (in the sense that the charge densities were the same for the two surfaces). This yields surface charge densities from $\sim +10^{-2}$ eÅ^{-2} (for the GlyR IC domain) to $\sim -10^{-3}$ eÅ^{-2} (for the nAChR EC domain).

The electrostatic consequences of these simple models of the remainder of the LGIC model were explored by calculation of electrostatic potential profiles along the cylinder (z) axis without the M2 α-helix bundle. For the nAChR α7 cylinder model, the net negative charge produced a well of depth $\sim -3RT$. This would be expected to enhance the cation selectivity of the channel (see next section). For the GlyR α1, the effect was more marked and in the opposite direction, with a potential barrier (for cations) of height $\sim 10RT$, due mainly to the IC domain. This would be expected to contribute to the observed anion selectivity of this channel.

These calculations are for (chick) nAChR α7 and (human) GlyR α1 sequences. One may ask what the average net charges on the three segments are when averaged across all nAChR α7 and across all GlyR α1 sequences. The average net charges are $+18.0$ (IC), -6.0 (TM), and -10.0 (EC) for α7 nAChRs; and $+58.0$ (IC), -4.0 (TM), and $+1.5$ (EC) for α GlyRs. Thus the overall pattern of charge distribution for the cylinder models is conserved within each receptor family.

There are a number of further assumptions implicit in these calculations on simple models. In particular, it is assumed that the pK_As of the surface residues are the same as for the isolated residues. However, as the inner radius of the cylinder is rather greater than that of the M2 α-helix bundle, it seems less likely a priori that perturbation of pK_A values such as that observed for the E $+20'$ residues of nAChR M2α7 will occur, especially as only within the M2 bundle are ionizable side chains likely to be found in relatively narrow rings. Overall, these calculations on a simple model suggest that the remainder of the LGIC model may play an important role in determining the electrostatic potential profile experienced by a permeant ion.

Combining the two models

Having shown that two regions of LGICs, the M2-extended α-helix bundle and the remainder of the molecule, may both contribute to ion selectivity, it is reasonable to ask what the combined effect of the two regions will be. The two parts of the model were docked together, and those atoms of the cylinder that overlapped in space with those of the M2-extended helix bundle were removed (with minor charge redistributions to maintain the overall net charges), to yield the model shown in Fig. 6 *A*. As the embedding of the M2-extended bundle in the irregular cylinder changed both the dielectric and charge environment of the helix bundle, it was necessary to recalculate the pK_A values for the ionizable residues (Table 1). To investigate the effect of simply embedding the M2-extended model in an irregular cylinder of low dielectric, a pK_A calculation in which no surface charge was present on the cylinder was performed. Compared to the M2-extended bundle (albeit in a bilayer-mim-

icking low dielectric slab), the main effect of the low-dielectric cylinder is to increase the pK_A values of the E + 20′ ring such that all five glutamates at the extracellular mouth of the pore would be protonated at neutral pH. Adding surface charge to the surfaces of the cylinder does not result in any major further changes in ionization states. Thus, when embedded in the irregular cylinder, the most likely ionization state of the M2-extended model is 1) D − 4′, fully ionized; 2) E −1′, fully ionized; 3) K0′, fully ionized; and 4) E +20′, 0% ionized (i.e., fully protonated).

Calculation of the electrostatic potential profile based on this combined model shows that the two components of the channel structure influence the overall potential profile in a nonadditive fashion (Fig. 6 *B*). Thus the overall potential well is of depth $\sim -7RT$. Using a Poisson-Nernst-Planck approach (Kienker et al., 1994; Woolley et al., 1997) to calculate single-channel current-voltage relationships, we have shown that such a profile is compatible with the observed single-channel conductance of the α7 nicotinic receptor (Adcock et al., manuscript in preparation). In passing, we note that wells/barriers of this magnitude are frequently encountered in rate theory analysis of ion channel permeation (Hille, 1992). Furthermore, as with the M2-extended model in the absence of the irregular cylinder, the potential well is skewed toward the C-terminal (intracellular) mouth of the channel. Such asymmetry of the potential profile with respect to the net voltage drop across the channel would be expected to lead to some degree of rectification in its current-voltage relationship. The relationship between the shape of the potential profile and that of the corresponding current-voltage relationship has been discussed in some detail by, e.g., Lear et al. (1997), and has been explored in preliminary calculations for the LGICs under discussion in the current paper (Adcock et al., manuscript in preparation).

It is useful to consider the components influencing the effect of the addition of the simple cylinder model to the M2 bundle model. If the nAChR M2α7 model is embedded in an uncharged simple cylinder model, then the effect of having the M2 charges within a low-dielectric cylinder is to increase the depth of the potential well from $\sim -3RT$ to $-5RT$. As discussed by, e.g., Hille (1992) and Klapper et al. (1986), such a "focusing" of the M2-generated electrostatic field by embedding in a low-dielectric environment was to be anticipated and may, indeed, be a general feature of a number of ion channels. The additional effect of the simple cylinder model on the profile is thus due to both the surrounding low-dielectric cylinder and to the assumption of the distribution of charge on the surrounding cylinder of protein—hence the nonadditivity in Fig. 6 *B*. This implies that both the shape and surface charge of a vestibule may contribute to the overall electrostatic potential profile of a channel.

For the GlyR M2α1 model the potential barrier is $\sim 4RT$ in height (see above). This is increased to $\sim 18RT$ if the M2 bundle is embedded in the outer cylinder (Fig. 7). Thus the remainder of the protein may make a significant contribution to the electrostatic potential profile (and hence the ion selectivity) of the GlyR. In particular, for the α1 GlyR the surface charge on the IC domain (mainly from the loop between M3 and M4; see Fig. 1 *A*) makes a major contribution to the electrostatic properties of the channel. For the GlyR we have not generated an M2-extended model. Examination of GlyR sequences reveals a proline residue at −2′, which would be expected to prevent an N-terminal extended helix from forming. This does not imply that residues N-terminal to M2 do not play a role in the electrostatics of GlyR, but rather that, as we cannot confidently predict the conformation of this region, it seems more reasonable to include such residues in the surface charge of the IC region of the irregular cylinder model for the remainder of the protein.

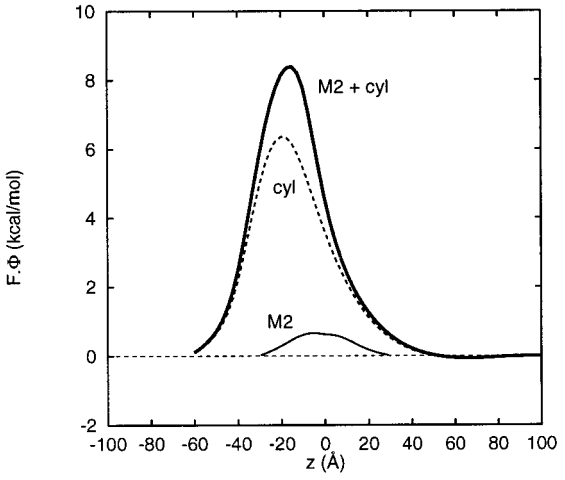

FIGURE 7 Electrostatic potential ($F\Phi$) profiles for GlyR M2α1 pore and irregular cylinder models: M2α1 model (no irregular cylinder) in its most likely ionization state (*thin solid line*); irregular cylinder model (no M2 helix bundle), with the net charge spread over both the inner and outer surfaces of the cylinder (*broken line*); M2α1 model embedded in the irregular cylinder model (*bold solid line*). The extent of the irregular cylinder is the same as in Fig. 6.

Appraisal of methodology

In this study we have applied continuum electrostatics calculations to analyze the potential profile along a detailed model of an ion channel. This work adds to a number of other studies of channel electrostatics (Chen and Eisenberg, 1993a,b; Chen et al., 1997; Hoyles et al., 1996; Levitt, 1991a,b; Partenskii and Jordan, 1992; Syganow and von Kitzing, 1995; von Kitzing and Soumpasis, 1996). There are several simplifying assumptions involved in our calculations. The first assumption is that continuum calculations may be applied to a microscopic system. Studies of water-soluble proteins using such methods have yielded useful insights (Sharp and Honig, 1990), lending confidence to the extension of this approach to ion channels. The second major limitation is that the Poisson-Boltzmann equation is an equilibrium treatment, and under physiological condi-

tions (and indeed any conditions where there is net movement of ions through a channel) the system is not at equilibrium. So the calculations presented here should perhaps be viewed as an approximation in which a channel experiences no transbilayer ionic concentration or electrostatic potential differences. Clearly, extending the present calculations to LGICs in a more physiological environment may require a more sophisticated theoretical treatment of nonequilibrium effects. Nevertheless, the approach of treating nonequilibrium steady-state problems as perturbations to the equilibrium problem is well established, based ultimately on the fluctuation-dissipation theorem (Glansdorf and Prigogine, 1971; Keizer, 1987). Perhaps more significant is the approximation in which the effect of ion-ion interactions is treated via the "Boltzmann" term in the Poisson-Boltzmann equation, as it would be in bulk electrolyte. The validity of this approach still has to be tested, and there are other approaches involving (for example) the explicit calculation of the time-averaged potential due to the steady-state redistribution of ions in the channel (Chen et al., 1997).

A somewhat more technical limitation is the use of the linearized Poisson-Boltzmann equation. As discussed by, e.g., Jordan et al. (1989), the use of this approximation, rather than the full (i.e., nonlinearized) equation, may lead to errors in estimation of potential profiles along the length of a channel. However, Weetman et al. (1997) suggest that the form of the results is unaffected by the exact method of calculation. We have compared the potential profiles calculated using the linearized and the full Poisson-Boltzmann equation for the M2α7 model. The depth of the well for the nonlinearized equation (results not shown) is a little less than that with the linearized version (see Fig. 3 *B*). In general, the nonlinear equation tends to give a smoother (i.e., small wells and barriers) potential profile than the linearized form. However, the difference is not marked compared to, e.g., the differences between the profiles for different members of the same ensemble of structures, and so we suspect that the main source of errors in our calculations does not lie in this assumption.

One limitation of our calculations of residue pK_As is that they are based on the unoccupied channel, i.e., in the absence of permeant ions. Of course, as, e.g., a cation passes through a ring of acidic side chains, it is likely that its presence will result in a transient shift in pK_A favoring their deprotonation. However, whereas the qualitative effect of such interactions may be stated simply, a rigorous quantitative treatment is rather more difficult. One suspects there may be a stochastic element to be taken into account, depending on the mean dwell time of the ion within the vicinity of the side chain ring compared to the mean dwell time of a proton on the side chain. A full treatment of such effects will require, e.g., molecular dynamics simulations of ion/pore/water interactions utilizing a force field that allows for dynamic protonation/deprotonation of side chains.

One other consideration is that we have limited our calculations of potential profiles to one dimension, i.e., along the axis of the pore. However, if the individual members of, e.g., a ring of glutamate side chains have different protonation states, then a cation moving through the pore would experience a force driving it off axis, toward the ionized side chains. This will need to be considered in future extensions of the theoretical treatment developed in this paper, which should combine the three-dimensional electrostatic field generated by the channel (and the transmembrane potential difference) in three dimensions with a simulation of the diffusive motion of anions and cations in this field. We note that approaches to this general problem have been discussed in some detail by, e.g., Chen et al. (1997). However, while remaining critically aware of the theoretical limitations to the approach adopted in this paper, the results have some value in enabling one to analyze the contributions of the various domains of LGICs to their mechanism of ion selectivity.

Implications

What are the implications of these studies? The first is that there is a complex interplay between the pore-lining region (the "selectivity filter") and the extramembrane regions (the "vestibules") of LGICs in governing the electrostatic potential experienced by an ion as it moves through a channel. To date much of the focus, both experimental and theoretical, has been on the immediate lining of the pore. However, from the results presented above it is evident that the remainder of the protein may play an equally important role, both in increasing the "local concentration" of the permeant ion at the mouth of the transmembrane pore, and in "focusing" the electrostatic field due to the pore per se. This may be one reason why more selective ion channels have evolved in most cases to be large membrane proteins, even though, as demonstrated by, e.g., antibiotic peptides (Sansom, 1993), a simple bundle of TM helices without any of the other regions will suffice to form a relatively nonselective ion channel. It is also interesting to note that in acetylcholine esterase the whole of the protein plays a role in generating an electrostatic field that guides acetylcholine down a channel-like entrance to the active site (Ripoll et al., 1993).

The models developed in this paper are relatively simple in the vestibular regions and are more "fine-grained" in the transmembrane region. As higher resolution experimental data emerge (Unwin, 1996), these models will improve in their detail. However, it is already evident that by combining electrostatic potential profiles from such models with estimates of the local dielectric constant (Sansom et al., 1997) and ion diffusion coefficients (Smith and Sansom, 1997a) within the pore region, it will be possible to calculate current-voltage relationships for single-ion channels (Chen et al., 1997; Kienker et al., 1994b; Woolley et al., 1997), thus enabling a physical description of a fundamental physiological process.

Our thanks to Nigel Unwin and Pierre Jean Corringer for valuable discussions concerning this work.

This investigation was supported by grants from the Wellcome Trust. Our thanks to the Oxford Centre for Molecular Sciences for access to computing facilities.

REFERENCES

Akabas, M. H., C. Kauffmann, P. Archdeacon, and A. Karlin. 1994. Identification of acetylcholine receptor channel-lining residues in the entire M2 segment of the α subunit. *Neuron.* 13:919–927.

Barnard, E. A. 1992. Receptor classes and the transmitter-gated ion channels. *Trends Pharmacol. Sci.* 17:368–374.

Bashford, D., and K. Gerwert. 1992. Electrostatic calculation of the pK_a values of ionisable groups in bacteriorhodopsin. *J. Mol. Biol.* 224: 473–486.

Bashford, D., and M. Karplus. 1990. pKa's of ionisable groups in proteins: atomic detail from a continuum electrostatic model. *Biochemistry.* 29: 10219–10225.

Bashford, D., and M. Karplus. 1991. Multiple-site titration curves of proteins: an analysis of exact and approximate methods for their calculation. *J. Phys. Chem.* 95:9556–9561.

Betz, H. 1990. Homology and analogy in transmembrane channel design: lessons from synaptic membrane proteins. *Biochemistry.* 29:3591–3599.

Bormann, J., O. P. Hamill, and B. Sakmann. 1987. Mechanism of anion permeation through channels gated by glycine and gamma-aminobutyric acid in mouse cultured spinal neurones. *J. Physiol. (Lond.).* 385: 243–286.

Brooks, B. R., R. E. Bruccoleri, B. D. Olafson, D. J. States, S. Swaminathan, and M. Karplus. 1983. CHARMM: a program for macromolecular energy, minimisation, and dynamics calculations. *J. Comp. Chem.* 4:187–217.

Brünger, A. T. 1992. X-PLOR Version 3.1. A System for X-Ray Crystallography and NMR. Yale University Press, New Haven, CT.

Changeux, J. P., J. I. Galzi, A. Devillers-Thiéry, and D. Bertrand. 1992. The functional architecture of the acetylcholine nicotinic receptor explored by affinity labelling and site-directed mutagenesis. *Q. Rev. Biophys.* 25:395–432.

Chen, D., and R. Eisenberg. 1993a. Charges, currents, and potentials in ionic channel of one conformation. *Biophys. J.* 64:1405–1421.

Chen, D., and R. Eisenberg. 1993b. Flux, coupling, and selectivity in ionic channels of one conformation. *Biophys. J.* 65:727–746.

Chen, D., J. Lear, and B. Eisenberg. 1997. Permeation through an open channel: Poisson-Nernst-Planck theory of a synthetic ionic channel. *Biophys. J.* 72:97–116.

Couturier, S., D. Bertrand, J.-M. Matter, M.-C. Hernandez, S. Bertrand, N. Millar, S. Valera, T. Barkas, and M. Ballivet. 1990. A neuronal nicotinic acetylcholine receptor subunit (alpha 7) is developmentally regulated and forms a homooligomeric channel blocked by alpha BTX. *Neuron.* 5:847–856.

Davis, M. E., J. D. Madura, B. A. Luty, and J. A. McCammon. 1991. Electrostatics and diffusion of molecules in solution: simulations with the University of Houston Brownian dynamics program. *Comput. Phys. Comm.* 62:187–197.

DiPaola, M., P. N. Kao, and A. Karlin. 1990. Mapping the alpha-subunit site photolabelled by the noncompetitive inhibitor [^{3}H]quinacrine azide in the active state of the nicotinic acetylcholine receptor. *J. Biol. Chem.* 265:11017–11029.

Dwyer, T. M., D. J. Adams, and B. Hille. 1980. The permeability of the endplate channel to organic cations in frog muscle. *J. Gen. Physiol.* 75:469–492.

Galzi, J. L., A. Devillers-Thiery, N. Hussy, S. Bertrand, J. P. Changeux, and D. Bertrand. 1992. Mutations in the channel domain of a neuronal nicotinic receptor convert ion selectivity from cationic to anionic. *Nature.* 359:500–505.

Glansdorf, P., and I. Prigogine. 1971. Thermodynamic Theory of Structure, Stability and Fluctuations. Wiley-Interscience, New York.

Grenningloh, G., V. Schmieden, P. R. Schofield, P. H. Seeburg, T. Siddique, T. K. Mohandas, C. M. Becker, and H. Betz. 1990. Alpha-subunit variants of the human glycine receptor—primary structures, functional expression and chromosomal localisation of the corresponding genes. *EMBO J.* 9:771–776.

Hille, B. 1992. Ionic Channels of Excitable Membranes, 2nd Ed. Sinauer Associates, Sunderland, MA.

Hol, W. G. J., P. T. van Duijnen, and H. J. C. Berendsen. 1978. The α-helix dipole and the properties of proteins. *Nature.* 273:443–446.

Hollmann, M., C. Maron, and S. Heinemann. 1994. N-Glycosylation site tagging suggests a three transmembrane domain topology for the glutamate receptor GluR1. *Neuron.* 13:1331–1343.

Hoyles, M., S. Kuyucak, and S. H. Chung. 1996. Energy barrier presented to ions by the vestibule of the biological membrane channel. *Biophys. J.* 70:1628–1642.

Hucho, F., U. Görne-Tschelnokow, and A. Strecker. 1994. β-Structure in the membrane-spanning part of the nicotinic acetylcholine receptor (or how helical are transmembrane helices?). *Trends Biochem. Sci.* 19: 383–387.

Hucho, F., V. I. Tsetlin, and J. Machold. 1996. The emerging three-dimensional structure of a receptor: the nicotinic acetylcholine receptor. *Eur. J. Biochem.* 239:539–557.

Huyghues-Despointes, B. M. P., J. M. Scholtz, and R. L. Baldwin. 1993. Effect of a single aspartate on helix stability at different positions in a neutral alanine-based peptide. *Protein Sci.* 2:1604–1611.

Imoto, K., C. Busch, B. Sakmann, M. Mishina, T. Konno, J. Nakai, H. Buyo, Y. Mori, K. Kukuda, and S. Numa. 1988. Rings of negatively charged amino acids determine the acetylcholine receptor channel conductance. *Nature.* 335:645–648.

Jackson, M. B., and J. L. Yakel. 1995. The 5-HT$_3$ receptor channel. *Annu. Rev. Physiol.* 57:447–468.

Jones, D. T., W. R. Taylor, and J. M. Thornton. 1994. A model recognition approach to the prediction of all-helical membrane protein structure and topology. *Biochemistry.* 33:3038–3049.

Jordan, P. C., R. J. Bacquet, J. A. McCammon, and P. Tran. 1989. How electrolyte shielding influences the electrical potential in transmembrane ion channels. *Biophys. J.* 55:1041–1052.

Karshikoff, A., V. Spassov, S. W. Cowan, R. Ladenstein, and T. Schirmer. 1994. Electrostatic properties of two porin channels from *Escherichia coli*. *J. Mol. Biol.* 240:372–384.

Keizer, J. 1987. Statistical Thermodynamics of Nonequilibrium Processes. Springer-Verlag, New York.

Kerr, I. D., R. Sankararamakrishnan, O. S. Smart, and M. S. P. Sansom. 1994. Parallel helix bundles and ion channels: molecular modelling via simulated annealing and restrained molecular dynamics. *Biophys. J.* 67:1501–1515.

Kienker, P. K., W. F. DeGrado, and J. D. Lear. 1994b. A helical-dipole model describes the single-channel current rectification of an uncharged peptide ion channel. *Proc. Natl. Acad. Sci. USA.* 91:4859–4863.

Kienker, P., G. Tomaselli, M. Jurman, and G. Yellen. 1994a. Conductance mutations of the nicotinic acetylcholine receptor do not act by a simple electrostatic mechanism. *Biophys. J.* 66:325–334.

Klapper, I., H. Hagstrom, R. Fine, K. Sharp, and B. Honig. 1986. Focusing of electric fields in the active site of copper superoxide dismutase: effects of ionic strength and amino-acid modification. *Proteins Struct. Funct. Genet.* 1:47–59.

Kraulis, P. J. 1991. MOLSCRIPT: a program to produce both detailed and schematic plots of protein structures. *J. Appl. Crystallogr.* 24:946–950.

Langosch, D., C. M. Becker, and H. Betz. 1990. The inhibitory glycine receptor: a ligand gated chloride channel of the central nervous system. *Eur. J. Biochem.* 194:1–8.

Langosch, D., K. Hartung, E. Grell, E. Bamberg, and H. Betz. 1991. Ion channel formation by synthetic transmembrane segments of the inhibitory glycine receptor—a model study. *Biochim. Biophys. Acta.* 1063: 36–44.

Lear, J. D., J. P. Schneider, P. K. Kienker, and W. F. DeGrado. 1997. Electrostatic effects on ion selectivity and rectification in designed ion channel peptides. *J. Am. Chem. Soc.* 119:3212–3217.

Lester, H. 1992. The permeation pathway of neurotransmitter-gated ion channels. *Annu. Rev. Biophys. Biomol. Struct.* 21:267–292.

Levitt, D. G. 1991a. General continuum theory for multi-ion channel. 1. Theory. *Biophys. J.* 59:271–277.

Levitt, D. G. 1991b. General continuum theory for multi-ion channel. 2. Application to acetylcholine channel. *Biophys. J.* 59:278–288.

Lim, C., D. Bashford, and M. Karplus. 1991. Absolute pKa calculations with continuum dielectric methods. *J. Phys. Chem.* 95:5610–5620.

Macdonald, R. L., and R. W. Olsen. 1994. GABAa receptor channels. *Annu. Rev. Neurosci.* 17:569–602.

Montal, M. 1995. Design of molecular function: channels of communication. *Annu. Rev. Biophys. Biomol. Struct.* 24:31–57.

Morr, J., N. Rundstrom, H. Betz, D. Langosch, and B. Schmitt. 1995. Baculovirus-driven expression and purification of glycine receptor alpha1 homo-oligomers. *FEBS Lett.* 368:495–499.

Nazaki, Y., and C. Tanford. 1967. Examination of titration behaviour. *Methods Enzymol.* 11:715–734.

Nilges, M., and A. T. Brünger. 1993. Successful prediction of the coiled coil geometry of the GCN4 leucine zipper domain by simulated annealing: comparison to the X-ray structure. *Proteins Struct. Funct. Genet.* 15:133–146.

Nutter, T. J., and D. J. Adams. 1995. Monovalent and divalent cation permeability and block of neuronal nicotinic receptor channels in rat parasympathetic ganglia. *J. Gen. Physiol.* 105:701–723.

Ortells, M. O., and G. G. Lunt. 1995. Evolutionary history of the ligand gated ion channel superfamily of receptors. *Trends Neurosci.* 18: 121–127.

Partenskii, M. B., and P. C. Jordan. 1992. Theoretical perspectives on ion-channel electrostatics—continuum and microscopic approaches. *Q. Rev. Biophys.* 25:477–510.

Ripoll, D. R., C. H. Faerman, P. H. Axelsen, I. Silman, and J. L. Sussman. 1993. An electrostatic mechanism for substrate guidance down the aromatic gorge of acetylcholine esterase. *Proc. Natl. Acad. Sci. USA.* 90:5128–5132.

Sankararamakrishnan, R., C. Adcock, and M. S. P. Sansom. 1996. The pore domain of the nicotinic acetylcholine receptor: molecular modelling and electrostatics. *Biophys. J.* 71:1659–1671.

Sansom, M. S. P. 1993. Structure and function of channel-forming peptaibols. *Q. Rev. Biophys.* 26:365–421.

Sansom, M. S. P., R. Sankararamakrishnan, and I. D. Kerr. 1995. Modelling membrane proteins using structural restraints. *Nature Struct. Biol.* 2:624–631.

Sansom, M. S. P., G. R. Smith, C. Adcock, and P. C. Biggin. 1997. The dielectric properties of water within model transbilayer pores. *Biophys. J.* 73:2404–2415.

Sharp, K. A., and B. Honig. 1990. Electrostatic interactions in macromolecules: theory and applications. *Annu. Rev. Biophys. Biophys. Chem.* 19:301–332.

Sitkoff, D., D. J. Lockhart, K. A. Sharp, and B. Honig. 1994. Calculation of electrostatic effects at the amino terminus of an alpha helix. *Biophys. J.* 67:2251–2260.

Smith, G. R., and M. S. P. Sansom. 1997a. Computer simulation of water and sodium ions in models of the nicotinic acetylcholine receptor. *J. Physiol. (Lond.).* 504P:P158.

Smith, G. R., and M. S. P. Sansom. 1997b. Molecular dynamics study of water and Na^+ ions in models of the pore region of the nicotinic acetylcholine receptor. *Biophys. J.* 73:1364–1381.

Stroud, R. M., M. P. McCarthy, and M. Shuster. 1990. Nicotinic acetylcholine receptor superfamily of ligand gated ion channels. *Biochemistry.* 29:11009–11023.

Syganow, A., and E. von Kitzing. 1995. Integral weak diffusion and diffusion approximations applied to ion transport through biological ion channels. *J. Phys. Chem.* 99:12030–12040.

Toyoshima, C., and N. Unwin. 1988. Ion channel of acetylcholine receptor reconstructed from images of postsynaptic membranes. *Nature.* 336: 247–250.

Unwin, N. 1989. The structure of ion channels in membranes of excitable cells. *Neuron.* 3:665–676.

Unwin, N. 1993. Nicotinic acetylcholine receptor at 9 Å resolution. *J. Mol. Biol.* 229:1101–1124.

Unwin, N. 1995. Acetylcholine receptor channel imaged in the open state. *Nature.* 373:37–43.

Unwin, N. 1996. Projection structure of the nicotinic acetylcholine receptor: distinct conformations of the α subunits. *J. Mol. Biol.* 257: 586–596.

Villarroel, A., S. Herlitze, M. Koenen, and B. Sakmann. 1991. Location of a threonine residue in the a-subunit M2 transmembrane segment that determines the ion flow through the acetylcholine receptor channel. *Proc. R. Soc. Lond. B.* 243:69–74.

von Kitzing, E., and D. M. Soumpasis. 1996. Electrostatics of a simple membrane model using Greens-function formalism. *Biophys. J.* 71: 795–810.

Weetman, P., S. Goldman, and C. G. Gray. 1997. Use of the Poisson-Boltzmann equation to estimate the electrostatic free energy barrier for dielectric models of biological ion channels. *J. Phys. Chem.* 101: 6073–6078.

Woolley, G. A., P. C. Biggin, A. Schultz, L. Lien, D. C. J. Jaikaran, J. Breed, K. Crowhurst, and M. S. P. Sansom. 1997. Intrinsic rectification of ion flux in alamethicin channels: studies with an alamethicin dimer. *Biophys. J.* 73:770–778.

Yang, A., M. R. Gunner, R. Sampogna, K. Sharp, and B. Honig. 1993. On the calculation of pKas in proteins. *Proteins Struct. Funct. Genet.* 15:252–265.